

Hydrogen Doping Induced $p_x \pm ip_y$ Triplet Superconductivity in Quasi-One-Dimensional $K_2Cr_3As_3$

Ming Zhang,^{1,*} Chen Lu,^{2,†} Yajiang Chen,¹ Yunbo Zhang,¹ and Fan Yang^{3,‡}

¹*Department of Physics, Zhejiang Sci-Tech University, Hangzhou, Zhejiang, 310018 P. R. China*

²*New Cornerstone Science Laboratory, Department of Physics,*

School of Science, Westlake University, Hangzhou 310024, Zhejiang, China

³*School of Physics, Beijing Institute of Technology, Beijing 100081, China*

Quasi-one-dimensional (Q1D) Cr-based pnictide $K_2Cr_3As_3$ has aroused great research interest due to its possible triplet superconducting pairing symmetry. Recent experiments have shown that incorporating hydrogen atoms into $K_2Cr_3As_3$ would significantly change its electronic and magnetic properties. Hence, it's necessary to investigate the impact of hydrogen doping in superconducting pairing symmetry of this material. Employing the hydrogen as a non-trivial electron-doping, our calculations show that, different from the p_z -wave obtained without hydrogen, the system exhibits $p_x \pm ip_y$ pairing superconductivity under specific hydrogen doping. Specifically, we adopt the random-phase-approximation approach based on a six-band tight-binding model equipped with multi-orbital Hubbard interactions to study the hydrogen-doping dependence of the pairing symmetry and superconducting T_c . Under the rigid-band approximation, our pairing phase diagram shows that the spin-triplet pairing state is dominated in the hydrogen-doping regime $x \in (0, 0.7)$. Particularly, the $T_c \sim x$ curve shows a peak at the 3D-quasi-1D Lifshitz transition point, and the pairing symmetry around this doping level is $p_x \pm ip_y$. The physical origin of this pairing symmetry is that the density of states is mainly concentrated at $k_x(k_y)$ with large momentum. Due to the three-dimensional character of the real material, this $p_x \pm ip_y$ -wave superconducting state possesses point gap nodes. We further provide experiment prediction to identify this triplet $p_x \pm ip_y$ -wave superconductivity.

I. INTRODUCTION

Since 2015, the discovery of the superconductivity in quasi-one-dimensional (Q1D) Cr-based compounds $A_2Cr_3As_3$ ($A = K, Rb, Cs$) has generated immediate and continued research interest [1–18]. These compounds consist of alkali-metal-atom-separated $[(Cr_3As_3)^{2-}]_\infty$ double-walled subnanotubes with the low-energy degrees of freedom dominated by the Cr $3d$ orbitals [19, 20], which are proposed to be strongly correlated [5, 8, 14, 21, 22, 24, 27, 30, 31], implying an electron-interaction-driven pairing mechanism. Evidence for unconventional SC in $K_2Cr_3As_3$ and its analogues [2–4] has been accumulated from various experiments [4–6, 8, 32, 33]. In particular, a novel spin-triplet pairing was theoretically proposed [19, 21–24], in accordance with the ferromagnetic spin fluctuations [8, 19]. Recently, the nuclear magnetic resonance (NMR) measurements of the Knight shift show spin triplet superconductivity behavior in $K_2Cr_3As_3$ [34]. Besides, spin relaxation rate study has revealed point nodes in the gap function [8, 18]. Therefore, superconducting pairing symmetry in this system could be $p_x \pm ip_y$ -wave. Such a state breaks time reversal symmetry and is consistent with zero-field muon spin resonance (μ SR) measurement that revealed evidence for a spontaneous appearance of a weak internal magnetic field below T_c [6].

Slightly after the synthesization of the $A_2Cr_3As_3$ (233) family, $A_1Cr_3As_3$ (133) was obtained by removing half of the A^+ ions and it exhibits superconductivity after doped with a certain percentage of hydrogen. Inspired by this, recent experiments intercalated hydrogen in $K_2Cr_3As_3$ to obtain

$K_2Cr_3As_3H_x$. Measuring its magnetic properties shows the presence of an AFM transition [44]. Note that, without hydrogen doping, the system has a ferromagnetic spin fluctuation [34, 38], and some theoretical calculations show that the superconductivity pairing symmetry is triplet p_z -wave [20–22]. Thus it is necessary to reconsider the superconducting pairing symmetry and magnetic fluctuations in this hydrogen-doped system.

The DFT-based calculations [44] show that the chemical reaction between $K_2Cr_3As_3$ and H_2 will form $K_2Cr_3As_3H$ with similar quasi-1D structure as that of $K_2Cr_3As_3$, but with the hydrogen atoms intercalated at the center of Cr octahedra in the $[(Cr_3As_3)^{2-}]_\infty$ subnanotubes. In the aspect of band structure [44], the role of the intercalated hydrogen atoms mainly lie in the rise of the Fermi energy E_F , besides modest distortions to the bands near E_F . Therefore, we can say that in $K_2Cr_3As_3H_x$, H has metallic bonding and acts as an electron donor. Furthermore the H concentration x in the material is experimentally tunable [44]. While the DFT results for $x = 1$ yield in-plane-antiferromagnetic ordered ground state [44], those for $x = 0$ suggest non-magnetic ground state with short-ranged ferromagnetic [21] spin fluctuations, which might mediate spin-triplet superconductor. Therefore, the phase diagram in $K_2Cr_3As_3H_x$ via tuning x is like those of the cuprates and the iron-pnictide superconductors wherein magnetic order states are usually found to be proximate to the SC, suggesting the relevance of the e-e interaction driven pairing mechanism. However, detailed theoretical studies about this phase diagrams are still missing.

In this article, we study the pairing symmetry of the $K_2Cr_3As_3H_x$ via the random-phase-approximation (RPA) approach [45–53], adopting the six-band tight-binding (TB) model proposed in Ref. [21]. Based on the band structure for $x = 0$, we use the rigid-band approximation to study the x -dependence of the pairing symmetry and the superconduct-

* mingz@zstu.edu.cn; These two authors contributed equally to this work.

† These two authors contributed equally to this work.

‡ yangfan_blg@bit.edu.cn

ing T_c in the regime $x \in (0, 0.7)$. Our results yield that the hydrogen doping induces a transition in the pairing symmetry of the system, from a p_z -wave type to a $p_x \pm ip_y$ -wave type. Particularly, when the $p_x \pm ip_y$ -wave leads the pairing symmetry, T_c reaches its peak. Investigating the Fermi surface (FS) we found this high T_c is obtained at the 3D-quasi-1D Lifshitz-transition doping level. To understand the physical origin of this superconducting phase transition, we investigate the distribution of the density of states (DOS) over the Fermi surface at different dopings. It shows that for dopings near 0.3, where the $p_x \pm ip_y$ -wave leads the pairing symmetry, the DOS reaches its peak at larger $k_x(k_y)$ compared with k_z . For other dopings where p_z -wave is the leading pairing symmetry, the DOS reaches its peak at larger k_z . We further discuss experimental verification of this $p_x \pm ip_y$ -wave superconducting state with point gap nodes.

The rest of this paper is organized as follows: In Sec. II, we construct the effective TB model and introduce the details of the RPA approach engaged in our calculations. In Sec. III, we analyze the magnetic fluctuations affecting the superconducting pairing through the dependence of the susceptibility on doping. In Sec. IV we calculate the dependence of superconducting pairing symmetry on hydrogen doping using the RPA approach. In Sec. V, we further propose the physical origin and experimental behaviors of the obtained $p_x \pm ip_y$ -wave superconductivity. A summary is given in Sec. VI together with some discussions about possible experimental implications.

II. MODEL AND APPROACH

A. The TB band structure

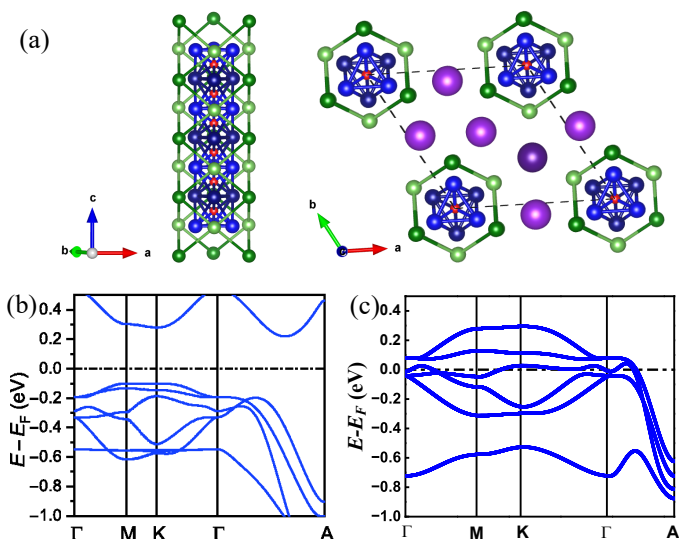


FIG. 1. (color online). Structural and band characterization of $K_2Cr_3As_3H_x$. (a) The crystal structure projected along b and c directions, respectively. (b) Band structure of $K_2Cr_3As_3H$ along the high-symmetry lines. (c) Band structure of $K_2Cr_3As_3$ in the same energy range as (b).

$K_2Cr_3As_3H_x$ crystallizes in a hexagonal lattice with $a = 10.0242(5)\text{\AA}$ and $c = 4.2501(8)\text{\AA}$, with a and c are 0.41% and 0.46% larger than the counterparts of $K_2Cr_3As_3$ [44]. The point group of this lattice is the same with the original lattice and it is D_{3h} , which includes a C_3 rotation about the z axis and a mirror reflection about the xy plane. The constituent atoms locate in the two crystalline planes with $z = 0$ and $z = 0.5$, as illustrated in Fig. 1(a). The hydrogen atoms are intercalated into the center of the CrAs tubes between the stacked CrAs layers, creating a chain of hydrogen centered in each tube. Compared with the $K_2Cr_3As_3H$'s low-energy band structure from the DFT calculations shown in Fig. 1(b), $K_2Cr_3As_3$ shows a similar shape, with only modest distortion near the Fermi level that is relatively decreased by about 0.3 eV (Fig. 1(c)). Therefore, the inserted hydrogen atoms in $K_2Cr_3As_3H_x$ can be well viewed as effective electron donors, consistent with previous results [44].

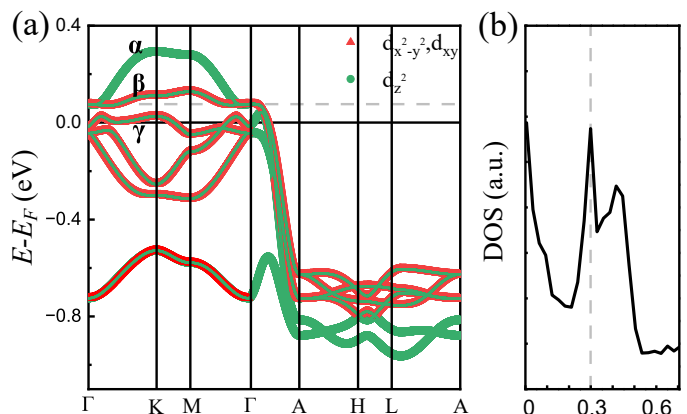


FIG. 2. (color online). Band structure (a) and density of energy state (b) of $K_2Cr_3As_3H_x$ from the six-band TB model. Hydrogen doping at the grey dashed line in (a) is 0.3.

As the IOP/CLK magnetic order calculated by DFT and a non-negligible out-of-plane coupling was estimated in Heisenberg model [44], we adopt a six-band TB model with both Cr1 and Cr2 involved which can reflect both the intra-chain and interchain magnetic properties of the system. This model was first proposed in Ref. [21]. Following Ref. [21], the obtained TB Hamiltonian in momentum space can be expressed as,

$$H_{TB} = \sum_{\mathbf{k}m\mu\nu\sigma} h_{\mu\nu}^{mn}(\mathbf{k}) c_{m\mu\sigma}^\dagger(\mathbf{k}) c_{n\nu\sigma}(\mathbf{k}), \quad (1)$$

Here $m/n = A, B$ labels sublattice, $\mu, \nu = 1, \dots, 3$ indicating the orbital indices, containing the d_{z^2} , $d_{x^2-y^2}$ and d_{xy} orbitals, and $\sigma = \uparrow, \downarrow$ labels spin. $c_{m\mu\sigma}^\dagger(\mathbf{k})$ ($c_{n\nu\sigma}(\mathbf{k})$) creates (annihilates) a spin- σ electron in the orbital μ (ν) in the m th (n th) sublattice with momentum \mathbf{k} . The elements of the $h(\mathbf{k})$ matrix of this six-band tight-binding model are given in Ref. [21].

Although the above-provided band structure and TB model are only accurately applicable to $K_2Cr_3As_3$, we take rigid-band approximation and adopt it to describe the band structure of $K_2Cr_3As_3H_x$, with only the chemical potential tuned

according to the variation of $x \in (0, 0.7)$. Note that, too high x might invalidate the rigid-band approximation as the band structure we adopt is for $x = 0$. Besides, the insulating state instead of SC is experimentally detected for x close to 1 [44].

Considering the presence of H deficiencies in experiments and a peak in the DOS at 0.3 doping during the rise in chemical potential as shown in Fig. 2(b), it is necessary to investigate how the FS are transformed in this process. We examined the doping dependence of FS and show three specific doping levels in Fig 3, i.e., $x = 0$ (Fig. 3(a₁)), $x = 0.3$ (Fig. 3(b₁)) and $x = 0.6$ (Fig. 3(c₁)). Although more doping dependence of FS have not been shown due to space limitations, one can find that the topology of the Fermi surface has significantly changed during doping. Particularly, a 3D-quasi-1D Lifshitz-transition occurred when doping around $x = 0.3$. Further, we marked the Van Hove Singularities' (VHS)'s k_z with k_c of each 3D FS, and made corresponding 2D cut as shown in the right column of Fig 3.

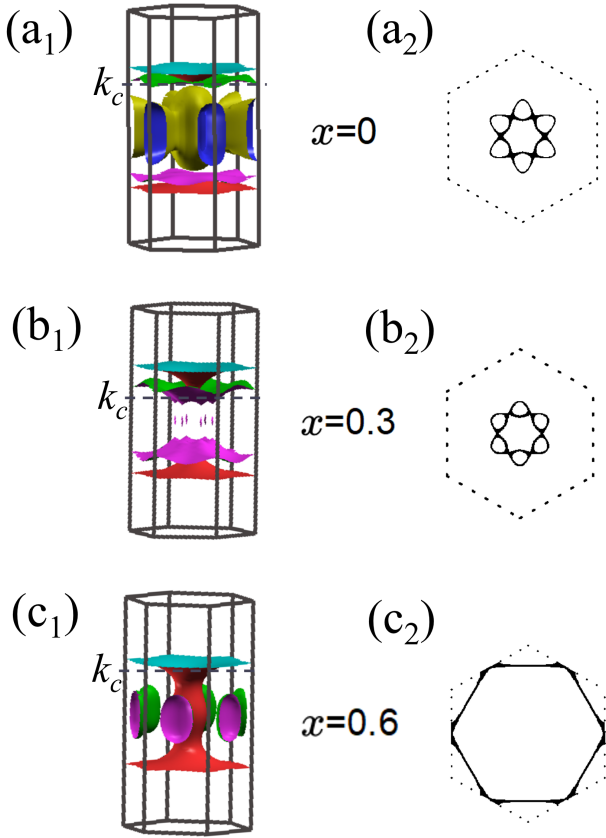


FIG. 3. (color online). 3D FSs and 2D cuts of the FSs on $k_z = k_c$ plane for $K_2Cr_3As_3H_x$ with typical doping levels (a) $x = 0$, (b) $x = 0.3$, and (c) $x = 0.6$ under the rigid-band approximation. Here k_c marked in 3D FSs is the corresponding k_c of 2D cuts.

B. The RPA approach

We first define the following bare susceptibility tensor in the normal state for the non-interacting case:

$$\chi_{pqst}^{(0)}(\mathbf{k}, \tau) \equiv \frac{1}{N} \sum_{\mathbf{k}_1 \mathbf{k}_2} \langle T_\tau c_p^\dagger(\mathbf{k}_1, \tau) c_q(\mathbf{k}_1 + \mathbf{k}, \tau) \times c_s^\dagger(\mathbf{k}_2 + \mathbf{k}, 0) c_t(\mathbf{k}_2, 0) \rangle_0, \quad (2)$$

Here $\langle \dots \rangle_0$ denotes the thermal average for the noninteracting system, T_τ denotes the imaginary time-ordered product, and the tensor indices $p, q, s, t = 1, \dots, 6$ denote the orbital-sublattice indices. Fourier transformed to the imaginary frequency space, the bare susceptibility can be expressed by the following explicit formulism:

$$\chi_{pqst}^{(0)}(\mathbf{k}, i\omega_n) = \frac{1}{N} \sum_{\mathbf{k}' \alpha \beta} \xi_t^\alpha(\mathbf{k}') \xi_p^{\alpha*}(\mathbf{k}') \xi_q^\beta(\mathbf{k}' + \mathbf{k}) \times \xi_s^{\beta*}(\mathbf{k}' + \mathbf{k}) \frac{n_F(\varepsilon_{\mathbf{k}'+\mathbf{k}}^\beta) - n_F(\varepsilon_{\mathbf{k}'}^\alpha)}{i\omega_n + \varepsilon_{\mathbf{k}'}^\alpha - \varepsilon_{\mathbf{k}'+\mathbf{k}}^\beta}. \quad (3)$$

where $\alpha, \beta = 1, \dots, 6$ are band indices, $\varepsilon_{\mathbf{k}}^\alpha$ and $\xi^\alpha(\mathbf{k})$ are the α -th eigenvalue (relative to the chemical potential μ_c) and eigenvector of the TB model, respectively, and n_F is the Fermi-Dirac distribution function.

To study superconductivity pairing phase diagram, we adopt the following extended Hubbard model Hamiltonian:

$$H = H_{TB} + H_{int} \\ H_{int} = U \sum_{i\mu} n_{i\mu\uparrow} n_{i\mu\downarrow} + V \sum_{i,\mu < \nu} n_{i\mu} n_{i\nu} + J_H \sum_{i,\mu < \nu} \left[\sum_{\sigma\sigma'} c_{i\mu\sigma}^+ c_{i\nu\sigma'}^+ c_{i\mu\sigma'} c_{i\nu\sigma} + (c_{i\mu\uparrow}^+ c_{i\mu\downarrow}^+ c_{i\nu\downarrow} c_{i\nu\uparrow} + h.c.) \right] \quad (4)$$

Here, the interaction parameters U , V , and J_H denote the intra-orbital, inter-orbital Hubbard repulsion, and the Hund's rule coupling (as well as the pair hopping) respectively, which satisfy the relation $U = V + 2J_H$.

When the Hubbard interaction in Eq. (4) is included, we can explicitly calculate the spin (s) and charge (c) susceptibilities following the standard multi-orbital RPA approach [45–53]. At the RPA level, the renormalized spin and charge susceptibilities of the system read

$$\chi^{(s,c)}(\mathbf{k}, i\omega_n) = [I \mp \chi^{(0)}(\mathbf{k}, i\omega_n) U^{(s,c)}]^{-1} \chi^{(0)}(\mathbf{k}, i\omega_n), \quad (5)$$

Here the nonzero elements $U_{\theta\xi}^{(s,c)\mu\nu}$ of $U^{(s,c)}$ satisfy $\mu, \nu, \theta, \xi \leq 3$ or > 3 simultaneously, which are as follow,

$$U_{\theta\xi}^{(s,c)\mu\nu} = \begin{cases} U(U), & \mu = \nu = \theta = \xi; \\ J_H(2V - J_H), & \mu = \nu \neq \theta = \xi; \\ J_H(J_H), & \mu = \theta \neq \nu = \xi; \\ V(2J_H - V), & \mu = \xi \neq \theta = \nu. \end{cases} \quad (6)$$

In Eq. (5), $\chi^{(s,c,0)}(\mathbf{k}, i\omega_n)$ and $U^{(s,c)}$ are operated as $6^2 \times 6^2$ matrices (see for example in Ref. [51]).

TABLE I. The ten possible pairing symmetries for $\text{K}_2\text{Cr}_3\text{As}_3\text{H}_x$ in the absence of SOC, among which five are spin-singlet while the rest are spin-triplet.

singlet	triplet
s	p_z
$(d_{x^2-y^2}, d_{xy})$	$(d_{x^2-y^2}, d_{xy}) \cdot p_z$
$(p_x, p_y) \cdot p_z$	(p_x, p_y)
$f_{x^3-3xy^2} \cdot p_z$	$f_{x^3-3xy^2}$
$f'_{y^3-3x^2y} \cdot p_z$	$f'_{y^3-3x^2y}$

Generally, repulsive Hubbard interactions suppress the charge susceptibility, but enhance the spin susceptibility [45–52, 54–57]. There is a critical interaction strength U_c , where the spin susceptibility diverges, implying the formation of spin density wave (SDW). At $U < U_c$, Cooper pairing may develop through exchanging spin and/or charge fluctuations. In particular, we consider Cooper pair scatterings both within and between the bands, hence both intra- and inter-band effective interactions $V^{\alpha\beta}(\mathbf{k}, \mathbf{k}')$ [21] (here $\alpha/\beta = 1, \dots, 6$ are band indices) are accounted for. From the effective interaction vertex $V^{\alpha\beta}(\mathbf{k}, \mathbf{k}')$, we obtain the following linearized gap equation near the superconducting T_c :

$$-\frac{1}{(2\pi)^3} \sum_{\beta} \oint_{FS} d^2 \mathbf{k}'_{\parallel} \frac{V^{\alpha\beta}(\mathbf{k}, \mathbf{k}')}{v_F^{\beta}(\mathbf{k}')} \Delta_{\beta}(\mathbf{k}') = \lambda \Delta_{\alpha}(\mathbf{k}). \quad (7)$$

Here the integration runs along the β - FS, $v_F^{\beta}(\mathbf{k}')$ is the corresponding Fermi velocity, and k'_{\parallel} is the component of \mathbf{k}' along the FS. Superconducting pairing in various channels emerge as the eigenstates of the above gap equation. The leading pairing $\Delta_{\alpha}(\mathbf{k})$ is given by the eigenstate corresponding to the largest eigenvalue λ . The critical temperature T_c is related to λ through $T_c \propto e^{-1/\lambda}$.

The eigenvector(s) $\Delta_{\alpha}(\mathbf{k})$ for each eigenvalue λ obtained from gap equation (7) as the basis function(s) forms an irreducible representation of the C_{6h} point group. In the absence of SOC, ten possible pairing symmetries are possible candidates for the system, which include five singlet pairings and five triplet pairings, as listed in Table I.

III. SUSCEPTIBILITY

The susceptibility tensor $\chi_{pqst}^{(0)}(\mathbf{k}, i\omega)$ defined on the above can be viewed as a matrix $\chi_{st}^{(0)pq}(\mathbf{k}, i\omega)$ by taking the combined pq indices as the row index and the combined st indices as the column index. In Fig. 4, we show the \mathbf{k} -dependence of the largest eigenvalue $\chi(\mathbf{k})$ of the zero-frequency susceptibility matrix $\chi_{st}^{(0)pq}(\mathbf{k}, i\omega_n = 0)$ for three different doping levels, i.e. $x = 0$ in (a)-(c), $x = 0.3$ in (d)-(f) and $x = 0.6$ in (g)-(i). Among these figures, the (a), (d) and (g) in the first row are along the high-symmetry lines in the Brillouin zone (BZ); the (b), (e) and (h) in the second row are on the $k_z = 0$ plane; and the (c), (f) and (i) in the third row are on the $k_z = \pi$ plane. Note that here $x = 0$ denotes $\text{K}_2\text{Cr}_3\text{As}_3$, $x = x_c = 0.3$ is the

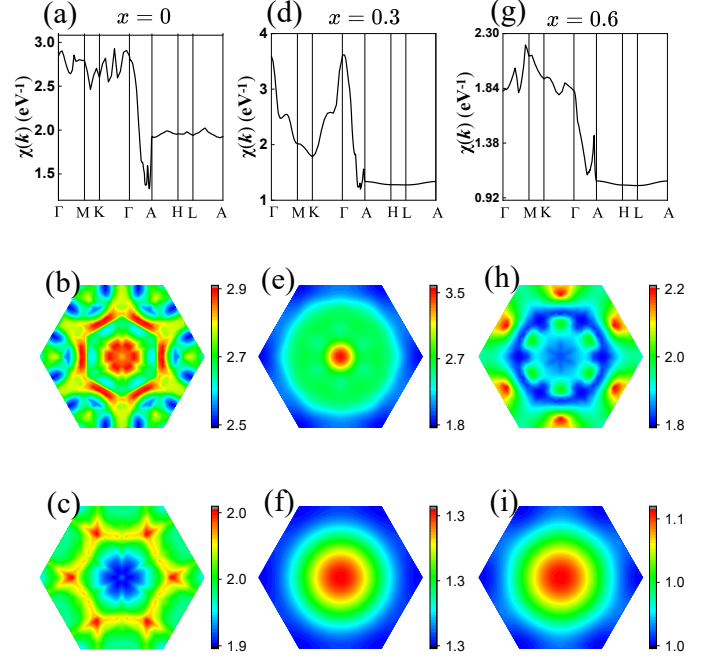


FIG. 4. (color online). The \mathbf{k} -space distribution of the largest eigenvalue $\chi(\mathbf{k})$ of the susceptibility matrix $\chi_{st}^{(0)pq}(\mathbf{k}, i\omega_n = 0)$ for (a)-(c) $\text{K}_2\text{Cr}_3\text{As}_3$, (d)-(f) $\text{K}_2\text{Cr}_3\text{As}_3\text{H}_{0.3}$ and (g)-(i) $\text{K}_2\text{Cr}_3\text{As}_3\text{H}_{0.6}$. From top to bottom are largest eigenvalue of the susceptibility matrix $\chi_{pqst}^{(0)}(\mathbf{k}, i\omega_n = 0)$ along the high-symmetry lines in the Brillouin zone, on the $k_z = 0$ plane and on the $k_z = \pi$ plane, respectively.

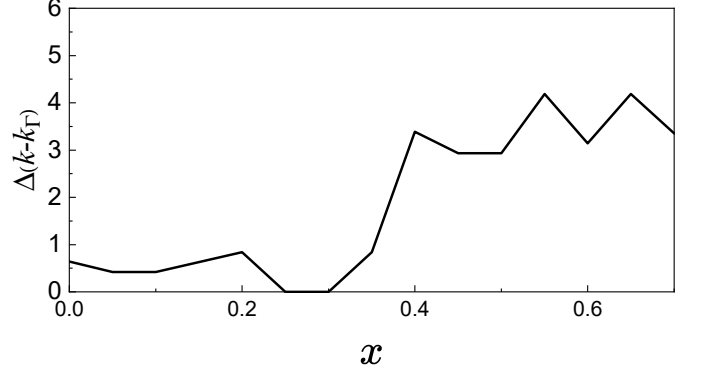


FIG. 5. (color online). The hydrogen-doping level x dependence of the distance between the \mathbf{k} and the Γ , where the maximum eigenvalue $\chi(\mathbf{k})$ of the susceptibility $\chi_{st}^{(0)pq}(\mathbf{k}, i\omega_n = 0)$ lies in.

3D-quasi-1D Lifshitz transition doping in our TB model, and the doping level $x = 0.6$ is close to the highest electron-doping level we considered.

Figure 4 illustrates two doping-dependent features for the distributions of the susceptibilities in the BZ. The first feature lies in that the location of the \mathbf{k}_M (which carries the strongest $\chi(\mathbf{k})$) are kept in the $k_z = 0$ plane from $x = 0$ to $x = 0.6$. We also calculated the largest eigenvalue $\chi(\mathbf{k})$ for other doping points and found that in the whole doping considered, the largest eigenvalue $\chi(\mathbf{k})$ of the $\chi_{st}^{(0)pq}(\mathbf{k}, i\omega_n = 0)$ always fall on

the $k_z = 0$ plane, implying an effective FM coupling between the equivalent Cr sites along the face-sharing Cr_6 octahedron chains. The second feature lies in that when the doping is less than 0.3, the maximum eigenvalue $\chi(k)$ located at Γ point, and when doping beyond 0.3, the k point of the maximum eigenvalue is no longer the Γ point. This is illustrated more clearly in Figure 5, from which we can see the k of the largest eigenvalue $\chi(k)$ is very close to Γ point when $x \leq 0.3$, and far from Γ when $x > 0.3$. That reflects the variation from interchain ferromagnetic correlations for $\text{K}_2\text{Cr}_3\text{As}_3$ to interchain antiferromagnetic correlations for $\text{K}_2\text{Cr}_3\text{As}_3\text{H}$. Note that, although there is an FM-AFM fluctuation transition in the interchain, there is always a ferromagnetic fluctuation in the intrachain, which is consistent with previous DFT results on $\text{K}_2\text{Cr}_3\text{As}_3\text{H}$ [44].

IV. PAIRING PHASE DIAGRAM

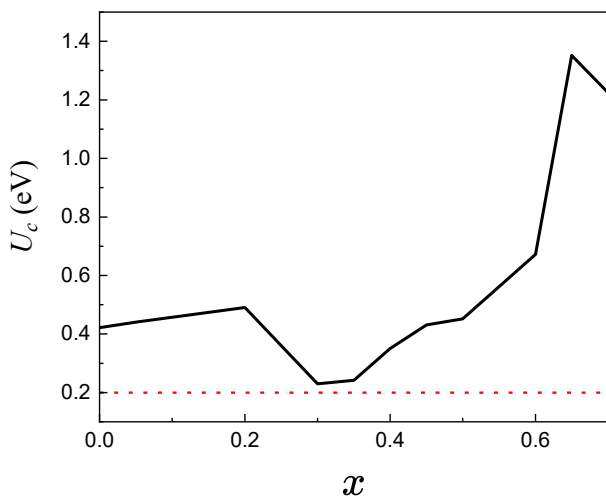


FIG. 6. (color online). Critical interaction U_c of the RPA spin susceptibility as a function of hole doping. In the main text, we adopt $U=0.2$ eV to calculate the pairing strength, in order to avoid magnetic instability.

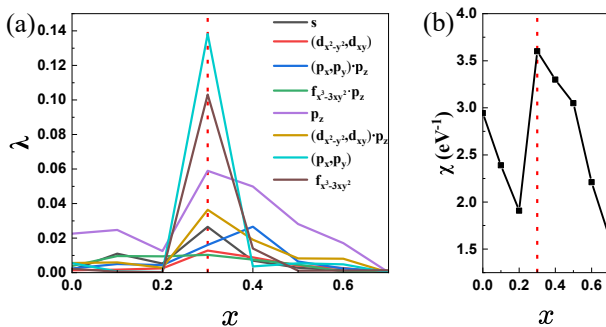


FIG. 7. (color online). (a) The largest pairing eigenvalues λ as function of x for eight pairing symmetries with relatively higher λ under $U = 0.2$ eV, $J_H = 0.2U$. (b) The doping dependences of χ_{Max} .

The doping dependences of the largest pairing eigenvalues λ for various pairing symmetries are shown in Fig. 7(a). Eight out of the ten possible pairing symmetries with relatively higher pairing eigenvalues are shown. The parameter settings are $J_H = 0.2U$ and $U = 0.2$ eV, satisfying $U < U_c$ in Fig. 6.

Three important results are provided by Fig. 7. Firstly, the triplet pairing is the leading pairing symmetry in the whole doping regime of $x \in (0, 0.7)$. When the doping x is close to 0, the leading pairing symmetry is triplet p_z -wave and it transforms to be (p_x, p_y) -wave when $x \in (0.2, 0.4)$. After x exceeds 0.4, the leading pairing symmetry transforms back to be p_z -wave. This result, combined with previous theories [21, 22, 24] and experiments [34], suggests that the SC in $\text{K}_2\text{Cr}_3\text{As}_3\text{H}_x$ is a robust triplet SC. From VHS in FS of these doping as shown in Fig. 3 we can find the VH momenta are located at time-reversal variant points which are called type-II VHS. It's pointed out [58–61, 64] that triplet SC would generally be favored near the type-II VHS. Secondly, the T_c peaks near the Lifshitz-transition point with $x \approx 0.3$, which is a DOS-peak according to Fig. 2. What's more, a comparison between Fig. 7(a) and (b) reveals the similarity between the $\lambda \sim x$ relation for the triplet SC and the $\chi \sim x$ relation. Combine Fig. 5 we can find that the k of the χ_{Max} in 0.3 doping is closest to the Γ point. As we know, the polarization vector of the magnetic order parameters close to Γ is favorable for ferromagnetic fluctuation. So the physical reason for the similarity between pairing symmetry and susceptibility lies in that the ferromagnetic fluctuation reflected by χ_Γ favors the formation of triplet SC. Thirdly, (p_x, p_y) -wave pairing occurs in this system due to hydrogen doping. This is a novel pairing symmetry of this system that we need to further analyze and understand.

V. THE $p_x \pm ip_y$ -WAVE SUPERCONDUCTIVITY

The leading pairing symmetry in Fig. 7 is p_z -wave in most doping levels we considered, and (p_x, p_y) -wave leading only in a very narrow doping level while its T_c is the largest in the entire doping level. Therefore, it is necessary to check this pairing phase diagram in the physical origin. Let's start with a more thorough investigation on the detailed DOS. Fix at different doping, we consider the distribution of DOS in three orthogonal axes of the first Brillouin zone. It shows significantly difference between 0.3 and other doping levels: Around 0.3 doping, DOS peaks at relatively large- $k_x(k_y)$ regime $k_x(k_y) \in (1.0, 1.2)$ and relatively small- k_z regime $k_z \approx 0.5$. But other doping cases are just opposite—the DOS-peak's $k_x(k_y)$ is relatively small and k_z is relatively large. In Fig. 8, we illustrate that for 0.1 doping case and 0.3 doping case. The reason why we focus on DOS-peak is that the regimes with relatively large DOS on the FS should be distributed with relatively large pairing gap amplitudes, so that the system can gain more energy from the superconducting condensation [62]. Besides, the distribution of p -waves is typically positively correlated with the value of k , e.g., p_z -wave pairing gap should be low in small- k_z regime and be high in

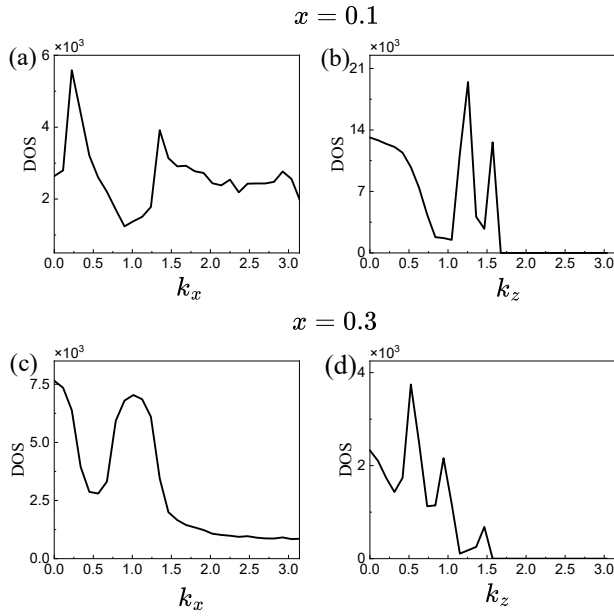


FIG. 8. The k dependence of DOS, where the doping is 0.1 in (a) and (b), and 0.3 in (c) and (d).

large- k_z regime. Therefore, the pairing-wave's symmetry depends on which direction the k of DOS-peak is larger. For 0.3 doping in this system, (p_x, p_y) -wave pairing is the leading pairing symmetry since the DOS-peak's $k_x(k_y)$ is relatively large in comparison with k_z as shown in Fig. 8(c) and (d). For other dopings, i.e. 0.1 doping, p_z -wave pairing is the leading pairing symmetry since the DOS-peak's k_z is relatively large in comparison with $k_x(k_y)$ as shown in Fig. 8(a) and (b). Thus, the pairing symmetry near 0.3 doping is (p_x, p_y) -wave, which is different from other doping, and the T_c maximum of (p_x, p_y) -wave is determined by the total DOS-peak as shown in Fig. 2(b) and 3D-quasi-1D lifshitz transition take place in this doping as shown in Fig. 3(b).

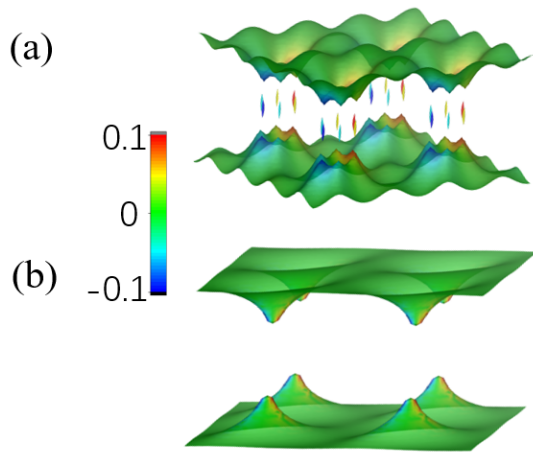


FIG. 9. (color online). The pairing gap functions shown on α FS (a) and β FS (b) for the $p_x \pm ip_y$ -SC with $x = 0.3$.

The distribution of the relative gap function of the obtained $p_x \pm ip_y$ -wave SC is shown on the α -, β - FSs for the Lifshitz-transition doping level $x = 0.3$ in Fig. 9 (a) and (b). While the α - FS at this doping is quasi-1D like planes almost parallel to the (k_x, k_y) -plane, the β - FS has six extremely thin tubular FS sheets in the middle of the quasi-1D like planes, which arise near $k_z = 0$. Figure 9 (a) and (b) show that this gap function is mirror symmetric about the σ_h , and changes sign when rotated 180 degrees about the z -axis, consistent with the p_x or p_y -wave pairing symmetry. The degenerate p_x - and p_y -wave pairings would always be mixed into the $p_x \pm ip_y$ form to lower the ground-state energy, as verified by some numerical results [63] and theoretical analysis [64, 65].

From Fig. 9 we can identify some slightly bright green gap zero points on the quasi-one-dimensional plane of the α and β Fermi surfaces, which also known as nodal-point. The triplet $p_x \pm ip_y$ -wave pairing state in 3D materials is so-called point-node superconductivity, as it forms points node with $k_x = k_y = 0$ on the Fermi plane. While the p_z -wave forms line node in the $k_z = 0$ plane, leading to line-node superconductivity. The experimental observable properties of point-node gap superconductivity and line-node gap superconductivity are the key criterion to distinguish $p_x \pm ip_y$ -wave and p_z -wave. Therefore, it is necessary to investigate $K_2Cr_3As_3H_x$'s temperature-dependent behavior of the various experimental observable properties, e.g., the specific heat $C_v(T)$, under different x . Here we perform a qualitative analysis of $p_x \pm ip_y$ -wave case, which will be discussed in detail in future studies.

Generally, $C_v(T)$ is:

$$\begin{aligned} C_v &= \frac{\partial}{\partial T} E = \frac{\partial}{\partial T} \sum_k \varepsilon_k^\alpha n_F(\varepsilon_k^\alpha) \\ &= \frac{\partial}{\partial T} \int \rho(\varepsilon) \varepsilon \frac{1}{e^{\beta\varepsilon} + 1} d\varepsilon \\ &= \int \rho(\varepsilon) \varepsilon \frac{\varepsilon e^{\beta\varepsilon} T^{-2}}{(e^{\beta\varepsilon} + 1)^2} d\varepsilon \end{aligned} \quad (8)$$

Here we take the boltzmann constant k_B as 1.

When $T \rightarrow 0$, $\beta \rightarrow \infty$, $\frac{e^{\beta\varepsilon}}{(e^{\beta\varepsilon} + 1)^2}$ is significantly nonzero only within the range of $\varepsilon \in (-k_B T, k_B T)$, leading to $\rho(\varepsilon) \propto \varepsilon^2$. This behavior is attributed to the presence of point nodes at $k_x = k_y = 0$ in the system. Therefore, as $T \rightarrow 0$, the specific heat is:

$$\begin{aligned} C_v &\propto \frac{1}{T^2} \int \varepsilon^4 \frac{e^{\beta\varepsilon}}{(e^{\beta\varepsilon} + 1)^2} d\varepsilon \\ &= \frac{1}{T^2} \int (\beta\varepsilon)^4 \frac{e^{\beta\varepsilon}}{(e^{\beta\varepsilon} + 1)^2} d\beta\varepsilon \times \frac{1}{\beta^5} \\ &\propto T^3 \int_{-\infty}^{\infty} x^4 \frac{e^x}{(e^x + 1)^2} dx \\ &\propto T^3 \end{aligned} \quad (9)$$

Similarly, the temperature-dependent behavior of other experimentally observable properties is as follows: the Knight shift $K_{ss} \propto T^2$, the NMR spin-relaxation rate $\frac{1}{T_1 T} \propto T^4$ and the superfluid density $\rho \propto T^2$ at sufficiently low temperature $T \ll T_c$, meanwhile, $C_v \propto T^2$, $K_{ss} \propto T$, $\frac{1}{T_1 T} \propto T^2$ and $\rho \propto T$

in p_z -wave superconductor. One can clearly judge which kind of superconducting symmetry in $\text{K}_2\text{Cr}_3\text{As}_3\text{H}_x$ by measuring the temperature-dependent behavior of the experimental observable properties listed above.

VI. DISCUSSION AND CONCLUSION

In conclusion, adopting six-band TB model which is specified in Ref. [21] equipped with the extended Hubbard interactions, we use the RPA approach to study the pairing state of the hydrogen doped $\text{K}_2\text{Cr}_3\text{As}_3$ under the rigid-band approximation. In the hydrogen-doping regime $x \in (0, 0.7)$, our RPA results yield the spin triplet pairing as the leading pairing symmetry. Specifically, when $x \in (0.3, 0.35)$, the leading pairing symmetry is the $p_x \pm ip_y$ -wave. This is the first theoretical calculations that achieves $p_x \pm ip_y$ -wave superconductivity in this system and hydrogen doping plays a key role. Since hydrogen-doped $\text{K}_2\text{Cr}_3\text{As}_3$ has already been successfully synthesized in experiments, we believe that by tuning the doping concentration, one can detect the $p_x \pm ip_y$ -wave superconductivity experimentally. Interestingly, recent NMR measurements of the Knight shift show spin triplet superconductivity behavior [34]. And the spin-lattice relaxation rate, $\frac{1}{T_1T} \propto T^4$ in the superconducting state, indicates the existence of point nodes in the superconducting gap function [8, 18]. These experimental properties indicate $p_x \pm ip_y$ -wave pairing symmetry in the system [34]. This may be due to the intercalation of a certain concentration of hydrogen in the experiment, as our hydrogen-doped results can support $p_x \pm ip_y$ -wave superconductivity.

Our pairing phase diagram shows that, when there is no hydrogen doping, i.e $\text{K}_2\text{Cr}_3\text{As}_3$, the triplet p_z -wave pairing is the leading pairing symmetry. Considering hydrogen as electron doping $x \in (0, 0.7)$, $p_x \pm ip_y$ -wave would be the leading pairing symmetry in $x \in (0.3, 0.35)$ doping. Noteworthy, in the doping levels that the $p_x \pm ip_y$ -wave leads the pairing symmetry, the T_c is the highest throughout the whole doping levels being considered. Careful investigation of the physical ori-

gin we found that the T_c peak is due to DOS peaking at the same doping. And the reason why the cooper pairs condensed a $p_x \pm ip_y$ -wave pairing is because the DOS at this doping is dense in the larger $k_x(k_y)$. However, in the doping region of p_z -wave pairing, we found DOS is dense in the larger k_z .

As for the magnetic properties, we found interchain magnetic fluctuation transforms from ferromagnetic fluctuation to antiferromagnetic fluctuation as x increases. Moreover, the maximum eigenvalue of susceptibility $\chi(\mathbf{k})$ always falls in the $k_z = 0$ plane throughout the whole doping level, which means that in-plane magnetism determines the overall magnetic performance of the system. Since it transforms into an antiferromagnetic spin fluctuation after the doping level becomes high, we can reasonably conclude that the magnetic order of $\text{K}_2\text{Cr}_3\text{As}_3\text{H}$ is antiferromagnetic, which is consistent with the recent experiment [44].

Note that, although the in-plane spin susceptibility transforms from ferromagnetic fluctuation to antiferromagnetic fluctuation, the intrachain spin susceptibility is always ferromagnetic fluctuation in $\text{K}_2\text{Cr}_3\text{As}_3\text{H}_x$. As we know, ferromagnetic spin fluctuations favor spin-triplet Cooper pairing. Combined with our findings that show triplet pairing is leading across all doping levels, we can infer that the enhancement of spin triplet superconductivity in this quasi-1D material is due to intrachain ferromagnetic fluctuations. Further, we suppose that intra-chain magnetic fluctuations play a key role in the superconducting pairing of all quasi-one-dimensional superconductors.

ACKNOWLEDGEMENTS

We are grateful to the stimulating discussions with Xianxin Wu. This work is supported by the Science Foundation of Zhejiang Sci-Tech University (ZSTU) (Grant No. 19062463-Y and No. 22062344-Y). F.Y. is supported by the National Natural Science Foundation of China under the Grants No. 12074031, No. 12234016.

-
- [1] J.-K. Bao, J.-Y. Liu, C.-W. Ma, Z.-H. Meng, Z.-T. Tang, Y.-L. Sun, H.-F. Zhai, H. Jiang, H. Bai, C.-M. Feng, Z.-A. Xu, and G.-H. Cao, *Superconductivity in Quasi-One-Dimensional $\text{K}_2\text{Cr}_3\text{As}_3$ with Significant Electron Correlations*, Phys. Rev. X **5**, 011013 (2015).
 - [2] Z.-T. Tang, J.-K. Bao, Y. Liu, Y.-L. Sun, A. Ablimit, H.-F. Zhai, H. Jiang, C.-M. Feng, Z.-A. Xu, and G.-H. Cao, *Unconventional Superconductivity in Quasi-One-Dimensional $\text{Rb}_2\text{Cr}_3\text{As}_3$* , Phys. Rev. B **91**, 020506(R) (2015).
 - [3] Z.-T. Tang, J.-K. Bao, Z. Wang, H. Bai, H. Jiang, Y. Liu, H.-F. Zhai, C.-M. Feng, Z.-A. Xu, G.-H. Cao, *Superconductivity in Quasi-One-Dimensional $\text{Cs}_2\text{Cr}_3\text{As}_3$ with Large Interchain Distance*, Sci. China Mater. **58**, 16 (2015).
 - [4] G.-M. Pang, M. Smidman, W.-B. Jiang, J.-K. Bao, Z.-F. Weng, Y.-F. Wang, L. Jiao, J.-L. Zhang, G.-H. Cao, and H.-Q. Yuan, *Evidence for Nodal Superconductivity in Quasi-One-Dimensional $\text{K}_2\text{Cr}_3\text{As}_3$* , Phys. Rev. B **91**, 220502 (2015).
 - [5] H.-Z. Zhi, T. Imai, F.-L. Ning, J.-K. Bao, and G.-H. Cao, *NMR Investigation of the Quasi-One-Dimensional Superconductor $\text{K}_2\text{Cr}_3\text{As}_3$* , Phys. Rev. Lett. **114**, 147004 (2015).
 - [6] D.-T. Adroja, A. Bhattacharyya, M. Telling, Y. Feng, M. Smidman, B. Pan, J. Zhao, A.-D. Hillier, F.-L. Pratt, and A.-M. Strydom, *Superconducting Ground State of Quasi-One-Dimensional $\text{K}_2\text{Cr}_3\text{As}_3$ Investigated Using μSR Measurements*, Phys. Rev. B **92**, 134505 (2015).
 - [7] T. Kong, S.-L. Budko, and P.-C. Canfield, *Anisotropic H_{c2} thermodynamic and transport measurements, and pressure dependence of T_c in $\text{K}_2\text{Cr}_3\text{As}_3$ single crystals*, Phys. Rev. B **91**, 020507(R) (2015).
 - [8] J. Yang, Z.-T. Tang, G.-H. Cao, and G.-Q. Zheng, *Ferromagnetic Spin Fluctuation and Unconventional Superconductivity in $\text{Rb}_2\text{Cr}_3\text{As}_3$ Revealed by ^{75}As NMR and NQR*, Phys. Rev. Lett. **115**, 147002 (2015).

- [9] F.-F. Balakirev, T. Kong, M. Jaime, R.-D. McDonald, C.-H. Mielke, A. Gurevich, P.-C. Canfield, and S.-L. Budko, *Anisotropy Reversal of the Upper Critical Field at Low Temperatures and Spin-Locked Superconductivity in $K_2Cr_3As_3$* , Phys. Rev. B **91**, 220505 (2015).
- [10] X.-F. Wang, C. Roncaglioli, C. Eckberg, H. Kim, J. Yong, Y. Nakajima, S.-R. Saha, P.-Y. Zavaliy, and J. Paglione, *Tunable electronic anisotropy in single-crystal $A_2Cr_3As_3$ ($A=K,Rb$) quasi-one-dimensional superconductors*, Phys. Rev. B **92**, 020508(R) (2015).
- [11] G. Pang, M. Smidman, W. Jiang, Y. Shi, J. Bao, Z. Tang, Z. Weng, Y. Wang, L. Jiao, J. Zhang, *Penetration depth measurements of $K_2Cr_3As_3$ and $Rb_2Cr_3As_3$* , J. Magn. Magn. Mater. **400**, 84 (2016).
- [12] G.-H. Cao, J.-K. Bao, Z.-T. Tang, Y. Liu, and H. Jiang, *Peculiar properties of Cr_3As_3 -chain-based superconductors*, Philos. Mag. **97**, 591 (2017).
- [13] D.-T. Adroja, A. Bhattacharyya, M. Smidman, A.-D. Hillier, Y. Feng, B. Pan, J. Zhao, M.-R. Lees, A.-M. Strydom, P.-K. Biswas, *Nodal superconducting gap structure in the quasi-one-dimensional $Cs_2Cr_3As_3$ investigated using μ SR measurements*, J. Phys. Soc. Jpn. **86**, 044710 (2017).
- [14] K.-M. Taddei, Q. Zheng, A.-S. Sefat, and C. Cruz, *Coupling of Structure to Magnetic and Superconducting Orders in Quasi-One-Dimensional $K_2Cr_3As_3$* , Phys. Rev. B **96**, 180506(R) (2017).
- [15] K. Zhao, Q.-G. Mu, T. Liu, B.-J. Pan, B.-B. Ruan, L. Shan, G.-F. Chen, Z.-A. Ren, *Superconductivity in Novel Quasi-One-Dimensional Ternary Molybdenum Pnictides $Rb_2Mo_3As_3$ and $Cs_2Mo_3As_3$* , [arXiv:1805.11577](https://arxiv.org/abs/1805.11577).
- [16] Q.-G. Mu, B.-B. Ruan, B.-J. Pan, T. Liu, J. Yu, K. Zhao, G.-F. Chen, and Z.-A. Ren, *Ion-Exchange Synthesis and Superconductivity at 8.6 K of $Na_2Cr_3As_3$ with Quasi-One-Dimensional Crystal Structure*, Phys. Rev. Materials **2**, 034803 (2018).
- [17] Q.-G. Mu, B.-B. Ruan, K. Zhao, B.-J. Pan, T. Liu, L. Shan, G.-F. Chen, Z.-A. Ren, *Superconductivity at 10.4 K in a Novel Quasi-One-Dimensional Ternary Molybdenum Pnictide $K_2Mo_3As_3$* , Sci. Bull. **63**, 952 (2018).
- [18] J. Luo, J. Yang, R. Zhou, Q.-G. Mu, T. Liu, Z.-A. Ren, C.-J. Yi, Y.-G. Shi, and G.-Q. Zheng, *Tuning the Distance to a Possible Ferromagnetic Quantum Critical Point in $A_2Cr_3As_3$* , Phys. Rev. Lett. **123**, 047001 (2019).
- [19] H. Jiang, G.-H. Cao, and C. Cao, *Electronic Structure of Quasi-One-Dimensional Superconductor $K_2Cr_3As_3$ from First-Principles Calculations*, Sci. Rep. **5**, 16054 (2015).
- [20] X. Wu, C. Le, J. Yuan, H. Fan, and J. Hu, *Magnetism in Quasi-One-Dimensional $A_2Cr_3As_3$ ($A=K,Rb$) Superconductors*, Chin. Phys. Lett. **32**, 057401 (2015).
- [21] X.-X. Wu, F. Yang, C.-C. Le, H. Fan, and J.-P. Hu, *Triplet p_z -Wave Pairing in Quasi-One-Dimensional $A_2Cr_3As_3$ Superconductors ($A=K,Rb,Cs$)*, Phys. Rev. B **92**, 104511 (2015).
- [22] L.-D. Zhang, X.-X. Wu, H. Fan, F. Yang, and J.-P. Hu, *Revisitation of Superconductivity in $K_2Cr_3As_3$ Based on the Six-Band Model*, Europhys. Lett. **113**, 37003 (2016).
- [23] A. Subedi, *Strong-coupling electron-phonon superconductivity in noncentrosymmetric quasi-one-dimensional $K_2Cr_3As_3$* , Phys. Rev. B **92**, 174501 (2015).
- [24] Y. Zhou, C. Cao, and F.-C. Zhang, *Theory for superconductivity in alkali chromium arsenides $A_2Cr_3As_3$ ($A=K,Rb,Cs$)*, Sci. Bull. **62**, 208 (2017).
- [25] J.-J. Miao, F.-C. Zhang, and Y. Zhou, *Instability of Three-Band Tomonaga-Luttinger Liquid: Renormalization Group Analysis and Possible Application to $K_2Cr_3As_3$* , Phys. Rev. B **94**, 205129 (2016).
- [26] H. Zhong, X.-Y. Feng, H. Chen, and J. Dai, *Formation of Molecular-Orbital Bands in a Twisted Hubbard Tube: Implications for Unconventional Superconductivity in $K_2Cr_3As_3$* , Phys. Rev. Lett. **115**, 227001 (2015).
- [27] X. Wu, F. Yang, S. Qin, H. Fan, and J. Hu, *Experimental Consequences of p_z -Wave Spin Triplet Superconductivity in $A_2Cr_3As_3$* , [arXiv:1507.07451](https://arxiv.org/abs/1507.07451).
- [28] R.-Y. Chen and N.-L. Wang, *Progress in Cr- and Mn-based superconductors: A key issues review*, Rep. Prog. Phys. **82**, 012503 (2018).
- [29] H. Jiang, G. Cao and C. Cao, *Electronic structure of quasi-one-dimensional superconductor $K_2Cr_3As_3$ from first-principles calculations*, Sci. Rep. **5**, 16054 (2015).
- [30] J.-J. Miao, F.-C. Zhang, and Y. Zhou, *Instability of Three-Band Tomonaga-Luttinger Liquid: Renormalization Group Analysis and Possible Application to $K_2Cr_3As_3$* , Phys. Rev. B **94**, 205129 (2016).
- [31] H. Zhong, X.-Y. Feng, H. Chen, and J. Dai, *Formation of Molecular-Orbital Bands in a Twisted Hubbard Tube: Implications for Unconventional Superconductivity in $K_2Cr_3As_3$* , Phys. Rev. Lett. **115**, 227001 (2015).
- [32] Y. Liu, J.K. Bao, H.K. Zuo, A. Ablimit, Z. T. Tang, C. M. Feng, Z.W. Zhu, and G. H. Cao, *Effect of impurity scattering on superconductivity in $K_2Cr_3As_3$* , Sci. China Phys. Mech. Astron. **59**, 657402 (2016).
- [33] H. K. Zuo, J. K. Bao, Y. Liu, J. H. Wang, Z. Jin, Z. C. Xia, L. Li, Z. A. Xu, J. Kang, Z. W. Zhu, and G. H. Cao, *Temperature and angular dependence of the upper critical field in $K_2Cr_3As_3$* , Phys. Rev. B **95**, 014502 (2017).
- [34] Y. Jie, L. Jun, C. J. Yi, Y. G. Shi, Y. Zhou, and G. Q. Zheng, *Spin-triplet superconductivity in $K_2Cr_3As_3$* , Sci. Adv. **7**, eabl4432 (2021).
- [35] P. A. Lee, N. Nagaosa, and X. G. Wen, *Doping a Mott insulator: Physics of high-temperature superconductivity*. Rev. Mod. Phys. **78** 17 (2006).
- [36] Q. M. Si, R. Yu, and E. Abrahams, *High-temperature superconductivity in iron pnictides and chalcogenides*, Nat. Rev. Mater. **1**, 16017 (2016).
- [37] Q.-G. Mu, B.-B. Ruan, B.-J. Pan, T. Liu, J. Yu, K. Zhao, G.-F. Chen, and Z.-A. Ren, *Superconductivity at 5 K in quasi-one dimensional Cr-based KCr_3As_3 single crystals*, Phys. Rev. B **96**, 140504(R) (2017).
- [38] G. Cuono, F. Forte, A. Romano, X. Ming, J. Luo, C. Autieri, and C. Noce, *Intrachain collinear magnetism and interchain magnetic phases in Cr_3As_3 -K-based materials*, Phys. Rev. B, **103**, 214406 (2021).
- [39] Y. Feng, X. Zhang, Y. Hao, A.-D. Hillier, D.-T. Adroja, and J. Zhao, *Magnetic ground state of KCr_3As_3* , Phys. Rev. B **99**, 174401 (2019).
- [40] K.-M. Taddei, L.-D. Sanjeeva, B.-H. Lei, Y.-H. Fu, Q. Zheng, D.-J. Singh, A.-S. Sefat, and C.-D. Cruz, *Tuning from frustrated magnetism to superconductivity in quasi-one-dimensional KCr_3As_3 through hydrogen doping*, Phys. Rev. B **100**, 220503(R) (2019).
- [41] J.-J. Xiang, Y.-L. Yu, S.-Q. Wu, B.-Z. Li, Y.-T. Shao, Z.-T. Tang, J.-K. Bao, and G.-H. Cao, *Superconductivity induced by aging and annealing in $K_{1-\delta}Cr_3As_3H_x$* , Phys. Rev. M **3**, 114802 (2019).
- [42] J.-J. Xiang, Y.-T. Shao, Y.-W. Cui, L.-P. Nie, S.-Q. Wu, B.-Z. Li, Z. Ren, T. Wu, and G.-H. Cao, *Superconductivity and phase separation in electrochemically hydrogenized $K_{1-\delta}Cr_3As_3H_x$* , Phys. Rev. M **4**, 124802 (2020).
- [43] S.-Q. Wu, C. Cao, and G.-H. Cao, *Lifshitz transition and nontrivial H-doping effect in the Cr-based superconductor*

- $KCr_3As_3H_x$, Phys. Rev. B **100**, 155108 (2019).
- [44] B.Z. Li, S.Q. Wu, J.J. Xiang, Q.Q. Zhu, L. Yi, C. Chao, G.-H. Cao, *Antiferromagnetic insulating state in quasi-one-dimensional $K_2Cr_3As_3H_x$* , Sci. China Phys. Mech. Astron. **66**, 237411 (2023).
- [45] T. Takimoto, T. Hotta, and K. Ueda, *Strong-Coupling Theory of Superconductivity in a Degenerate Hubbard Model*, Phys. Rev. B **69**, 104504 (2004).
- [46] K. Yada and H. Kontani, *Origin of the Weak Pseudo-gap Behaviors in $Na_{0.35}CoO_2$: Absence of Small Hole Pockets*, J. Phys. Soc. Jpn. **74**, 2161 (2005).
- [47] K. Kubo, *Pairing Symmetry in a Two-Orbital Hubbard Model on a Square Lattice*, Phys. Rev. B **75**, 224509 (2007).
- [48] K. Kuroki, S. Onari, R. Arita, H. Usui, Y. Tanaka, H. Kontani, and H. Aoki, *Unconventional Pairing Originating from the Disconnected Fermi Surfaces of Superconducting $LaFeAsO_{1-x}F_x$* , Phys. Rev. Lett. **101**, 087004 (2008).
- [49] S. Graser, T.-A. Maier, P.-J. Hirschfeld and D.-J. Scalapino, *Near-Degeneracy of Several Pairing Channels in Multiorbital Models for the Fe Pnictides*, New J. Phys. **11**, 025016 (2009).
- [50] T.-A. Maier, S. Graser, P.-J. Hirschfeld and D.-J. Scalapino, *d -Wave Pairing from Spin Fluctuations in the $K_xFe_{2-y}Se_2$ Superconductors*, Phys. Rev. B **83**, 100515(R) (2011).
- [51] F. Liu, C.-C. Liu, K. Wu, F. Yang and Y. Yao, *$d + id'$ Chiral Superconductivity in Bilayer Silicene*, Phys. Rev. Lett. **111**, 066804 (2013).
- [52] C.-C. Liu, L.-D. Zhang, W.-Q. Chen and F. Yang, *Chiral SDW and $d + id$ superconductivity in the magic-angle twisted bilayer graphene*, Phys. Rev. Lett. **121**, 217001 (2018).
- [53] L.-D. Zhang, X.-M. Zhang, J.-J. Hao, W. Huang, and F. Yang, *Singlet s^\pm -wave pairing in quasi-one-dimensional ACr_3As_3 ($A=K, Rb, Cs$) superconductors*, Phys. Rev. B **99**, 094511 (2019).
- [54] S. Raghu, A. Kivelson and D.-J. Scalapino, *Superconductivity in the Repulsive Hubbard Model: An Asymptotically Exact Weak-Coupling Solution*, Phys. Rev. B **81**, 224505 (2010).
- [55] D. J. Scalapino, *A common thread: The pairing interaction for unconventional superconductors*, Rev. Mod. Phys. **84**, 1383 (2012).
- [56] W. Kohn and J.-M. Luttinger, *New Mechanism for Superconductivity*, Phys. Rev. Lett. **15**, 524 (1965).
- [57] W. Cho, R. Thomale, S. Raghu and S.-A. Kivelson, *Band structure effects on the superconductivity in Hubbard models*, Phys. Rev. B **88**, 064505 (2013).
- [58] H. Yao, and F. Yang, *Topological odd-parity superconductivity at type-II two-dimensional van Hove singularities*, Phys. Rev. B **92**, 035132 (2015).
- [59] T.-X. Ma, F. Yang, H. Yao, and H.-Q. Lin, *Possible triplet $p+ip$ superconductivity in graphene at low filling*, Phys. Rev. B **90**, 245114 (2014).
- [60] Z.-Y. Meng, F. Yang, K.-S. Chen, H. Yao, and H.-Y. Kee, *Evidence for spin-triplet odd-parity superconductivity close to type-II van Hove singularities*, Phys. Rev. B **91**, 184509 (2015).
- [61] L.-D. Zhang, F. Yang, and Y.-G. Yao, *Itinerant ferromagnetism and $p+ip$ superconductivity in doped bilayer silicene*, Phys. Rev. B **92**, 104504 (2015).
- [62] J. Hu, H. Ding, *Local antiferromagnetic exchange and collaborative Fermi surface as key ingredients of high temperature superconductors*, Sci Rep **2**, 381 (2012)
- [63] C. Lu, L. D. Zhang, X. Wu, F. Yang, J. Hu, *$d + id$ chiral superconductivity in a triangular lattice from trigonal bipyramidal complexes.*, Phys. Rev. B, **97**, 165110 (2018).
- [64] X. Chen, Y. Yao, H. Yao, F. Yang, J. Ni, *Topological $p+ip$ superconductivity in doped graphene-like single-sheet materials BC_3 .*, Phys. Rev. B, **92**, 174503 (2015).
- [65] Y.B. Liu, Y. Zhang, W.Q. Chen, and F. Yang, *High-angular-momentum topological superconductivities in twisted bilayer quasicrystal systems.*, Phys. Rev. B, **107**, 014501 (2023).